OPTOELECTRONICS AND ADVANCED MATERIALS – RAPID COMMUNICATIONS Vol. 17, No. 11-12, November-December 2023, p. 502-511

Simulation of electronic processes in multilayer polymer light emitting diodes based on Ph-PPV as emitting layer

ALIASGHAR AYOBI*
Department of Physics, Bojnourd Branch, Islamic Azad University, Bojnourd, Iran

This paper investigates the mechanisms affecting on the electrical properties of polymer light-emitting diodes (PLEDs) with the structure of Indium tin oxide (ITO) /poly(para-phenylenevinylene) (Ph-PPV)/Mg in steady state condition. For this purpose, ATLAS SILVACO package, Poole-Frankel mobility model and Langevin recombination model are employed. With using this physical models based simulator, the performance of these devices with inserting 4,4',4"-tris{N,(3-methylphenyl)-N-phenylamino}-triphenylamine (m-MTDATA),m-MTDATA/ N,N'-diphenyl-N,N'-di(3-methylphenyl)-1,1' biphenyl-4,4'-Diamine (TPD) and m-MTDATA/ N,N'-biphenyl-N,N'-bis-(1-naphenyl)-[1,1'-biphthyl]4,4'-diamine (NPB) as organic hole transport layers(HTLs) and tris(8-hydroxyquinolinato)aluminum(Alq_3) as organic electron transport layer(ETL) is investigated. These layeres lead to the balance of the electron and hole currents,appropriate zone for recombination of charge carriers, improvement of the recombination rate, modification of the singlet exciton density profile and luminance amplification of these devices. The numerical framework used in this package is based on a 1-D time–independent drift–diffusion model and NEWTON method that in which a set of coupled, non-linear, partial differential equations are solved for simulating of the device operation.

(Received January 4, 2023; accepted December 4, 2023)

Keywords: Polymer light-emitting diode (PLED), Exciton, Luminance, Current Density, Recombination Rate

1. Introduction

The first investigations about electroluminescence of organic materials and organic light- emitting diodes (OLEDs) have been reported in the 1963 and 1970 respectively. But due to the low luminescence efficiency, these devices have not been used [1-2]. In 1977, with investigations carried out by Heeger et al., it was revealed that a thin film of poly acetylene can turns into a conductor under oxidization reaction with iodine vapor [3]. The first OLED devices based on tris(8-hydroxyquinolinato) aluminum (Alq_3) organic material as emitting layer have been fabricated by Tang and Vanslyke in 1987 [4]. Also, after the discovery of electroluminescence properties of some conjugated polymers at the Cambridge University in 1990, most extensive research efforts are concentrated on light-emitting device technologies. The reason is as follow: Their using in fabrication of displays and solid state light sources is important and they have interesting properties such as lower voltage for operation, lower power utilization for light emission, clarification, inexpensiveness and lightness [5,6]. For optimization of the device performance, it is essential to understand their physical mechanisms including charge carriers injection from electrodes to organic material, charge carriers transportation in organic layers and their recombination through the simulation process [4, 7]. In multi-layer devices, due to the existence of extra organic(polymeric) layers, the mobility of charge carriers and their injection rates are balanced that lead to the shift of recombination zone away from the electrodes and reduction of the luminescence quenching [8, 9]. The simulation process has three main advantages: first, the cost of a simulation process is much lower than performing experiments, Second, the consumed time for optimization in a simulation method is much lower than performing experiment and third, it provides information that their measuring is difficult or impossible [10, 11]. For solving the physical models,three main numerical methodes have been introduced in the literature: The first method, named as Monte Carlo algorithm considers the site energies as a random variables leading to hopping processes on a microscopic level. This method is very time consuming so that usually is used to characterization of carriers transport in the bulk of organic materials [12]. The second method,named as hopping transport, solves master equations [13,14]. In the third method named as drift-diffusion model, nonlinear coupled partial differential equations describe the injection, transport, and recombination of charge carriers. This method has been investigated by different researchers in the past few years that has led to the several electronic models consist of Poisson's Equation, continuity equation and transport equations [15-17]. In this work, with considering third method and ATLAS SILVACO package, the electronic properties of the multilayer polymer light- emitting diodes (PLEDs) including current density-voltage, luminescent power-voltage, Langevin recombination rate and singlet

exciton density profile has been investigated in the steady-state.

2. Simulation model

In this section, the numerical models that are used for simulating of the PLED devices have been introduced. There are different transport models such as the drift-diffusion model, the Energy Balance Transport model and the hydrodynamic model that have been derived by applying approximations to the Boltzmann Transport Equations [18, 19]. However, the numerical framework used in this paper is based on a 1-D and time–independent drift–diffusion model without considering trapped charge carriers. The basic equations of this model are as follows:

$$\frac{d^2\psi}{dx^2} = -\frac{q}{\varepsilon}\,(\text{p-n}) \tag{1}$$

$$\frac{d}{dx}\left(-\mu_n n\frac{d\psi}{dx} + D_n\frac{dn}{dx}\right) = R \tag{2}$$

$$\frac{d}{dx}\left(+\mu_p p\frac{d\psi}{dx} + D_p\frac{dp}{dx}\right) = R \tag{3}$$

In these equations, ψ denotes the electrostatic potential, ε is the product of the relative permittivity ε_r and the vacuum permittivity ε_0, R is the recombination rate, μ_n and μ_p are the electrons and holes mobility, n and p denotes the density of mobile electrons and holes respectively and D_n and D_p are the electrons and holes diffusion coefficients. It has been specified that the contacts with injection barriers lower than 0.3 eV are considered as Ohmic contact. In this simulation, the injection barriers are higher than 0.3 eV, therefore the contacts are Schottky type with $\varphi_b = \chi_c + E_g - \varphi_1$ as hole injection barrier and $\varphi_b = \varphi_2 - \chi_c$ as electron injection barrier. In these equations, φ_1 and φ_2 are work functions of the anode and cathode respectively and χ_c and E_g are electron affinity and band gap of the polymer respectively [20, 21]. In these contacts the surface potential is given by the following relation:

$$\Psi_s = \chi_c + \frac{E_g}{2q} + \frac{kT_L}{2q}ln\frac{N_c}{N_v} - \varphi + V_{applied} \tag{4}$$

That in which N_c and N_v are the conduction and valence band densities of states, φ is the work function of contact and T_L is the temperature. In this paper, the multilayer structures have been investigated that in which, materials with different molecular energy levels and different charge mobility have been separated from each other by internal interfaces. Therefore it is essential to consider alternative current density expressions for electrons and holes at these interfaces [22, 23]:

$$J_n = qv_n(1+\delta)\left[n_a - n_b exp\left(\frac{-\Delta E_c}{kT_L}\right)\right] \tag{5}$$

$$J_p = (-q)v_p(1+\delta)\left[p_a - p_b exp\left(\frac{-\Delta E_v}{kT_L}\right)\right] \tag{6}$$

In these equations, q is the magnitude of electron charge, δ represents the contribution due to thermionic field emission (tunneling), k is Boltzmann's constant, J_n and J_p are the electron and hole current densities from the "b" region to the "a" region and ΔE_c and ΔE_v are the conduction band energy changes and valance band energy changes going from the "b'' region to the "a" region respectively. In this study, the tunneling mechanisms are ignored, therefore the tunneling coefficient δ will be zero. Also v_n and $v_p$defined as below represent the electron and hole thermal velocities:

$$v_n = \frac{A_n T_L^2}{qN_c} \tag{7}$$

$$v_p = \frac{A_p T_L^2}{qN_v} \tag{8}$$

That in which, A_n and A_p are the Richardson constants of electrons and holes.

It is necessary to notice to the fact that in low electric fields, the mobility of charge carriers is constant, but with increasing electric field, it does not remain constant and according to Poole-Frankel mobility model changes with temperature (T) and applied electric field (E):

$$\mu = \mu_0^* \exp\left(-\frac{\Delta}{kT}\right)\exp\left(\sqrt{E/E_0}\right) \tag{9}$$

In this equation, μ_0^*, Δ , E=-dψ/dx and E_0 are mobility in the limit of zero field and infinite temperature, effective activation energy, electric field and the characteristic field of the materials respectively. Also the recombination rate of charge carriers is given with the Langevin bimolecular recombination rate model [24-26]:

$$R = \frac{q}{\varepsilon}(\mu_n + \mu_p)np \tag{10}$$

Since the organic materials used in this study are in non degenerate state, therefore the classical Einstein relation and Boltzmann approximation for carrier density are used:

$$\frac{D}{\mu} = \frac{kT}{q} \tag{11}$$

$$n = n_i exp\left(\frac{q(\psi-\varphi_n)}{kT}\right) \tag{12}$$

$$p = p_i exp\left(\frac{q(\varphi_p-\psi)}{kT}\right) \tag{13}$$

$$n_i = p_i = \sqrt{N_C N_V}\exp\left(\frac{-E_g}{2kT}\right) \tag{14}$$

$$E_F = -q\varphi = \frac{E_C+E_V}{2} + \left(\frac{kT}{2}\right)\ln\left(\frac{N_V}{N_C}\right) \tag{15}$$

In these relations, n_i is the intrinsic carrier density and φ_n and φ_p are the quasi-Fermi potentials for electrons and holes respectively. The recombination of electrons and holes in the emitting layer leads to the generation of

singlet and triplet excitons. However since in this paper we deal with fluorescent emitting material so only singlet excitons needs to be considered and triplet excitons will decay non raditively. Also the excitons diffusion length (L) can be considered as the emission zone width. To study of the luminance spatial evolution, it is essential to consider the one-dimensional continuity equation for singlet excitons (in steady state) as follows:

$$\gamma R + D_s \frac{d^2 S}{dx^2} - \frac{S}{\tau} = 0 \qquad (16)$$

In which S is the singlet exciton density, γ = 1/4 is probability of the singlet excitons formation due to spin statistics, τ is the excitons lifetime and Ds = L^2/τ is the exciton diffusion constant [27].

3. Structures and simulation parameters

The PLED structures that are simulated in this manuscript are as follows:

Device A: ITO/Ph-PPV (60 nm)/Mg.Ag

Device B:ITO/m-MTDATA (40 nm)/Ph-PPV (60 nm)/Mg.Ag

Device C: ITO / m-MTDATA (20 nm) /TPD (20 nm)/Ph-PPV(60 nm)/Mg.Ag

Device D: ITO / m-MTDATA (20 nm) /NPB (20 nm)/ Ph-PPV(60 nm)/Mg.Ag

Device E: ITO/Ph-PPV (60 nm) / Alq_3 (20 nm)/Mg.Ag

Device F: ITO / m-MTDATA(20 nm) / Ph-PPV (60 nm)/Alq_3 (20 nm)/ Mg.Ag

In these devices, the organic materials,4,4',4"-tris{N,(3-methylphenyl)-N-phenylamino}-triphenylamine(m-MTDATA), N,N'-diphenyl-N,N'-di(3-methylphenyl)-1,1' biphenyl-4,4'-Diamine(TPD) and N,N'-biphenyl-N,N'-bis-(1-naphenyl)-[1,1'-biphthyl]4,4'-diamine (NPB) are used as hole transport layers (HTLs). The fluorescent polymer, poly(para-phenylenevinylene) (Ph-PPV), also known as "super yellow (SY)" is used as light emitting layer (EML) and the organic material of tris-(8-hydroxy-quinoline) Aluminum(Alq_3) is used as electron transport layer (ETL). It is essential to notice that, the difference between the work functions of electrodes and highest occupid molecular orbital (HOMO) or lowest unoccupid molecular orbital (LUMO) leveles of organic materials leads to the formation of potential energy barriers at the interfaces between electrodes and organic materials. For this purpose, it is essantial to use of the metals with low work function such as Mg.Ag as cathode and the metals with high work function such as ITO as anode for reduction of energy barriers. Also for obtaining more accuracy in simulation results,the structures need to be meshed perfectly. The band structure and essential parameters of the materials for simulating of the devices are presented in Fig. 1 and Table 1 respectively [28-39].

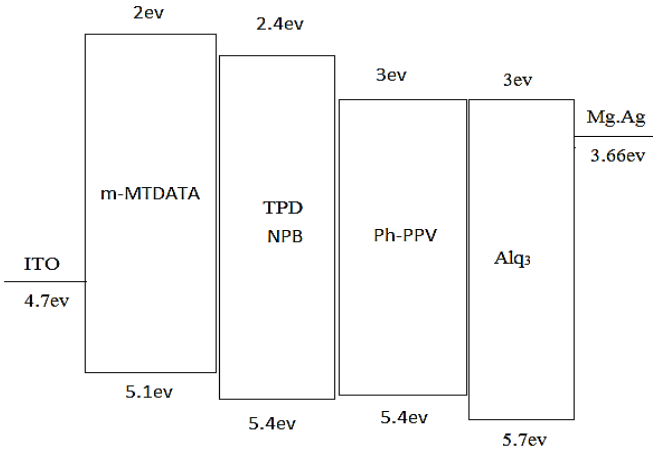

Fig. 1. Band structure of the investigated OLEDs

Table 1. Essential parameters of the materials

material	ε_r	N_{LUMO} (cm^{-3})	N_{HOMO} (cm^{-3})	E_g (ev)	χ_c (ev)	$\mu_{0,p}(\frac{cm^2}{Vs})$	$E_{0,p}(\frac{V}{cm})$	$\mu_{0,n}(\frac{cm^2}{Vs})$	$E_{0,n}(\frac{V}{cm})$	$\tau(ns)$	L(nm)	φ(eV)
m-MTDATA	3.5	2×10^{21}	2×10^{21}	3.1	2	4.79×10^{-6}	8.7×10^{4}	4.7910^{-8}	8.7×10^{4}	10	10	
TPD	3	1×10^{21}	1×10^{21}	3	2.4	6.1×10^{-4}	4.44×10^{5}	6.1×10^{-6}	4.44×10^{5}	1.89	17	
NPB	3.2	1×10^{21}	1×10^{21}	3	2.4	2.6×10^{-4}	4×10^{5}	5.28×10^{-6}	4×10^{5}	3.5	5	
Ph-PPV	3	1×10^{21}	1×10^{21}	2.4	3	1×10^{-7}	35000	1×10^{-111}	7000	0.4	4	
Alq_3	3	1×10^{19}	1×10^{19}	2.7	3	1.5×10^{-9}	7.1×10^{4}	1.5×10^{-7}	7.1×10^{4}	16	8	
ITO												4.7
Mg.Ag												3.66

4. Numerical solution methods

Different numerical methods are used for simulating of the organic semiconductor devices that are as follows: (a) decoupled (GUMMEL) method, (b) fully coupled (NEWTON) method and (c) BLOCK method that in which some equations are fully coupled while others are de-coupled. In this manuscript, the operation of the devices is

modeled with a set of coupled, nonlinear, partial differential equations by using of the NEWTON method (ATLAS SILVACO package). The numerical solutions of these equations are obtained by calculating the values of unknowns on a mesh of pointes under the following process:

At the first step, the continuous model is converted to a discrete non-linear algebraic system. In continuation, this system is solved iteratively starting from an initial guess until convergence criteria are obtained. The applied voltage to each electrode is started from zero bias and is increased step by step (with limited step sizes) for calculation of the current density and luminance power in each bias point [40-43].

5. Simulation results and discussions

It is possible to fabricate high quality multilayer structures with organic materials due to the existance of vander waals type bonds in these materials "a relatively weak force in comprision with covalent bonds in inorganic semiconductors". In PLEDs the recombination rate of electrons and holes is determined by the interfacial charge densities (langevin recombination model). This quantity is very important for performance of these devices, because of the dependence of singlet exciton density, luminance power and light output to this quantity. Thus, for optimization of these devices performance, it is essantial to balance the electron and hole currents for limitting of the carriers recombination at the best emitting zone. For this purpose, the performance of the PLED device with the structure of ITO/Ph-PPV/Mg.Ag is optimized with inserting m-MTDATA, m-MTDATA/TPD and m-MTDATA/NPB as HTLs and Alq_3 as ETL. In fact, organic materials used as HTL and ETL can lead to the balance of charge carrieres injection and transportation and increasing of the luminance efficiency. The simulation results (the recombination rate, distribution of the singlet exciton density and charge carriers concentration) for different PLED devices are presented in Figs. 2, 3 and 4 respectively. The distribution of the singlet excitons is an important factor for performance of the PLED devices so that the emission zone is defined as the 1/e width of the singlet exciton density profile. In device A, the accumulation of charge carriers and their recombination occurs in all regions of the emitting layer, the exciton profile has a uniform distribution in all regions of the emitting layer while the recombination rate and singlet exciton density reduce to zero at the contacts. In devices B, C and D, the electron blocking properties of the HTLs and hole blocking properties of the EML lead to the accumulation and recombination of electrons and holes at the HTL-EML interfaces. In these devices, the singlet exciton density profile has a maximum in these interfaces with a tail in other regions that means emission zone is located in these interfaces. However in m-MTDATA/TPD interface for device C and m-MTDATA/NPB interface for device D there are another significant recombination rate and a maximum for singlet exciton density profile that result from accumulation of electrons and holes in these interfaces. In devices E and F, the hole blocking properties of ETL, the electron blocking properties of HTL and the electron and hole blocking properties of EML lead to the accumulation of holes and electrons at EML-ETL interface for device E and at HTL-EML and EML-ETL interfaces for device F.

Therefore in these devices, the charge carriers recombination rate curve and singlet exciton density profile curve have the highest values in these regions while reduces in other regions (the emission zone is located in these regions). In comparison between different devices at a given voltage, the charge carriers recombination rate curve and singlet exciton density profile curve have the highest values for device B and these curves have the lowest values for device A. In fact for device A, the lower injection barrier of electrons (0.66 eV) in comparison with holes (0.7 eV) lead to the unbalanced injection and transport of electrons and holes. In conclusion the performance of this device would be the worst in comparison with other devices. The insertion of m-MTDATA, m-MTDATA/TPD and MTDATA/NPB as HTL between the anode and Ph-PPV layer also Alq_3 as ETL between the Ph-PPV layer and cathode in other devices increases the hole and electron concentrations. This increases lead to the improvement of carrier balance and better performance for these devices in comparison with device A. In devices C and D, with double HTL (m-MTDATA/TPD or m-MTDATA/NPB) the injection and transport of electrons and holes is unbalanced which lead to worse performance for these devices with respect to device B. Thus for these devices, the Langevin recombination rate and singlet exciton density profile are lower than those for device B. The insertion of Alq_3 as ETL in device E and both Alq_3 and m-MTDATA as ETL and HTL in device F causes to the unbalanced electron and hole injection and transport with respect to devices B, C and D. Therefore, the Langevin recombination rate and singlet exciton density profile in these devices are reduced with respect to devices B, C and D. In comparison between devices E and F, the situation of charge carrier balance in device F with m-MTDATA as HTL and Alq_3 as ETL is better than device E with only m-MTDATA as HTL. Therefore, the Langevin recombination rate and singlet exciton density profile in device F are higher than those for device E.

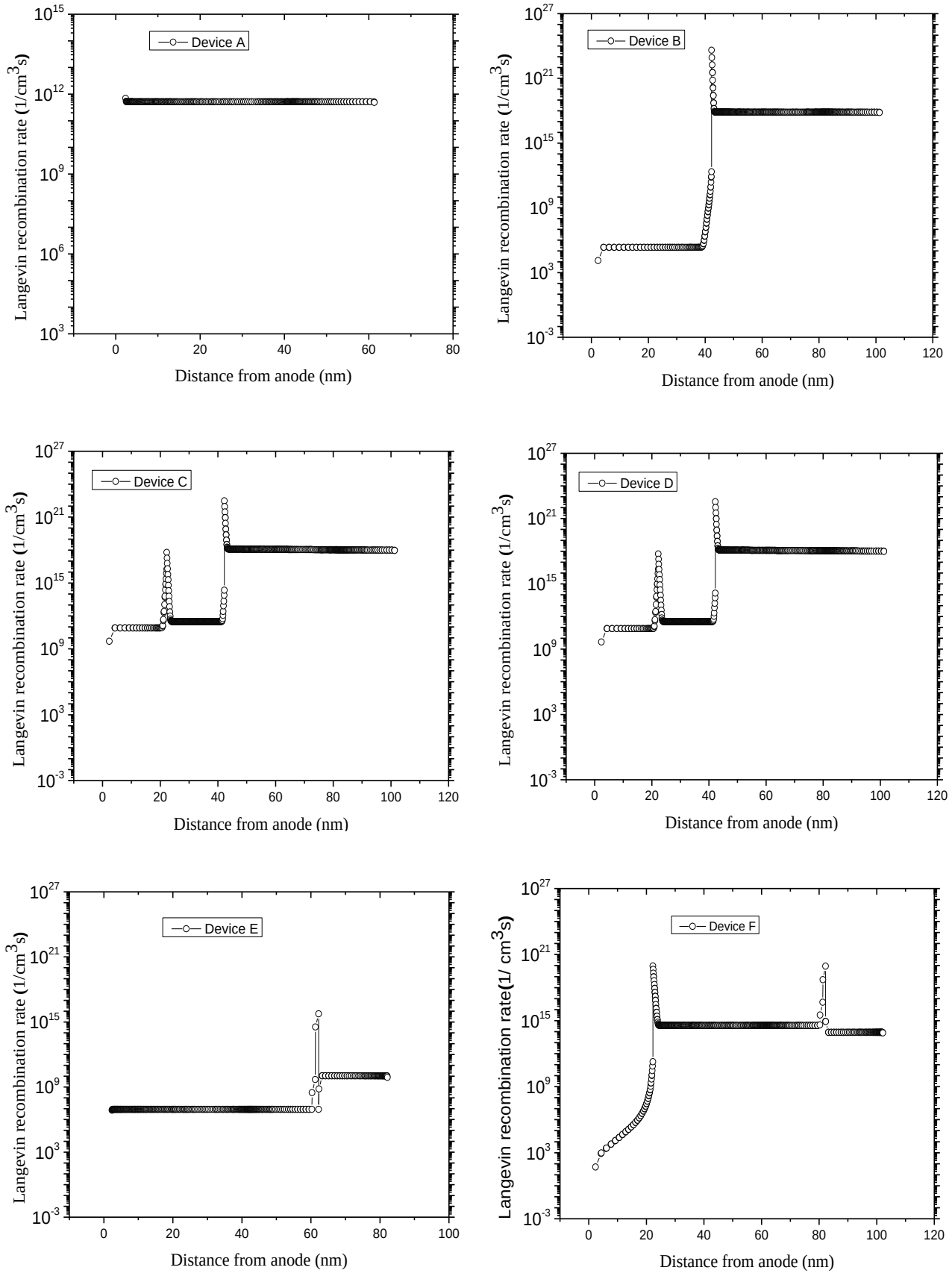

Fig. 2. Langevin recombination rate versus distance from anode

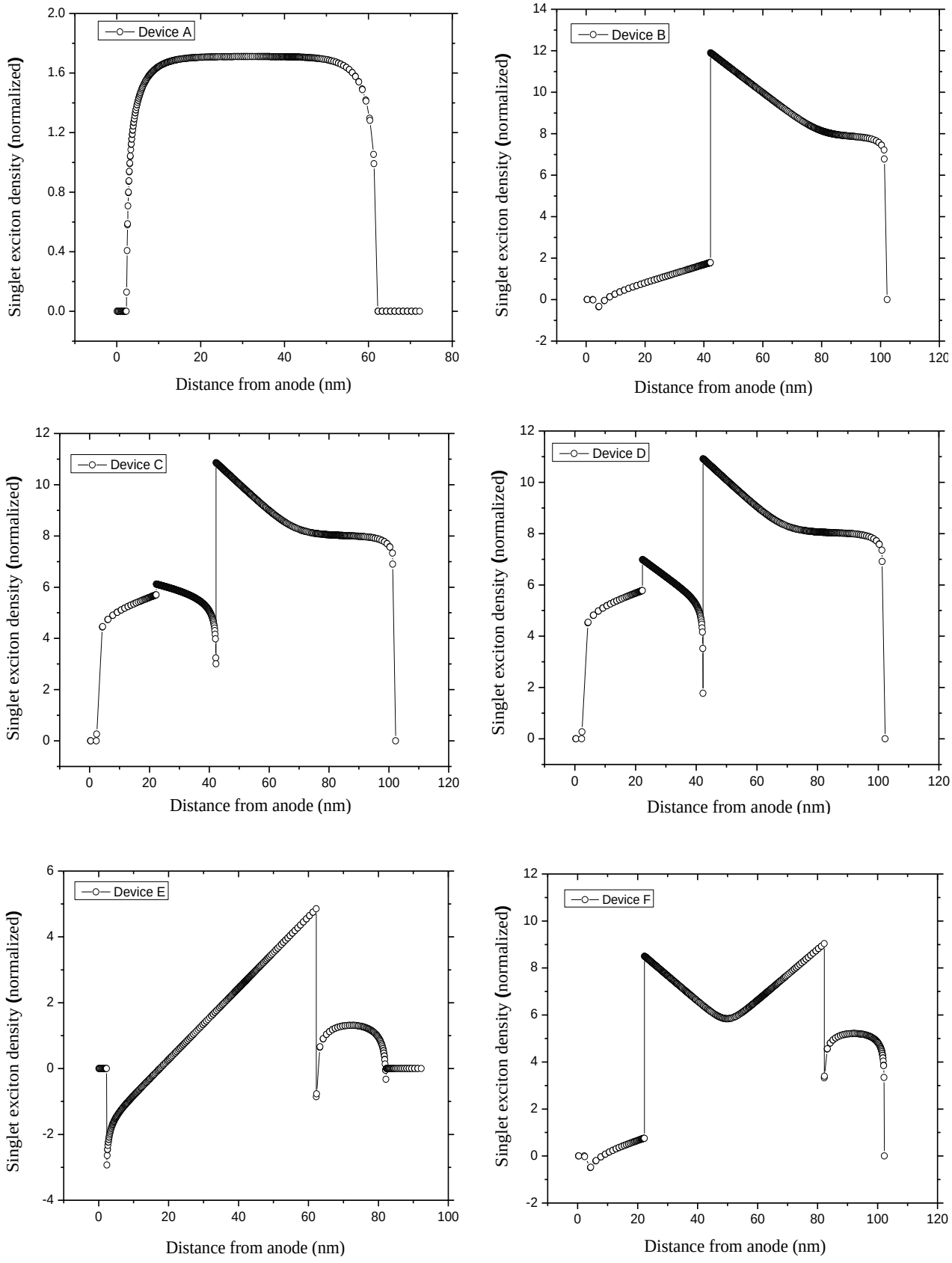

Fig. 3. Singlet exciton density versus distance from anode

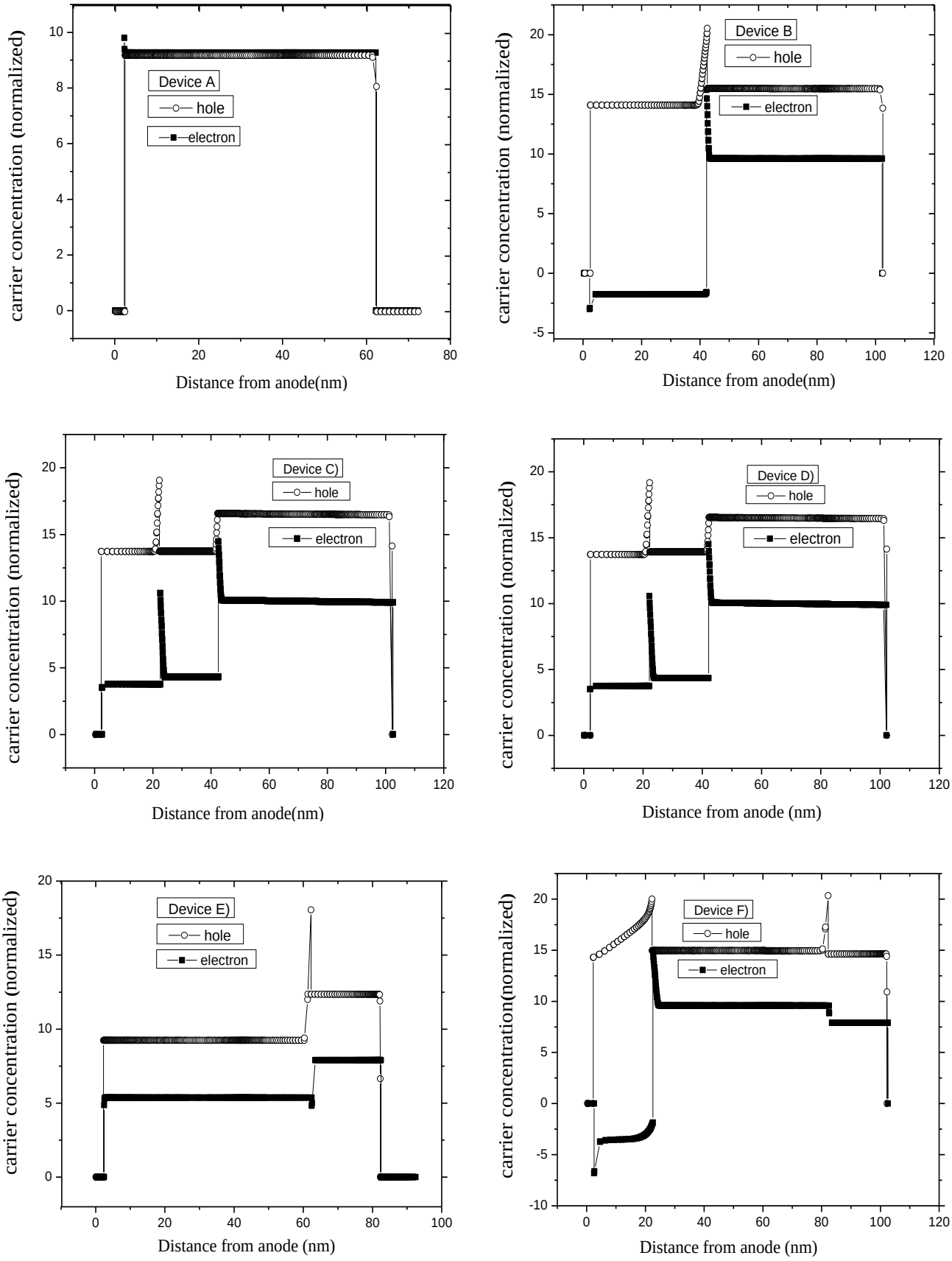

Fig. 4. Carrier concentration versus distance from anode

The simulated current density-voltage and Luminance-voltage characteristics for different devices involved in this manuscript have been showed in Figs. 5 and 6 respectively. It is clear from these graphs that the insertion of m-MTDATA, m-MTDATA/TPD and m-MTDATA/NPB as HTL(intermediate layer between the anode and Ph-PPV layer) respectively in devices B, C and D lead to the improvement of hole injection due to the HOMO level of m-MTDATA (5.1 eV). In conclusion, the driving voltage at a given current density and operating voltage at a given luminescent power reduce that lead to the improvement of carrier balance, anode current and luminescent power with respect to device A. In comparison between devices B, C and D, due to the higher mobility of holes in TPD and NPB with respect to m-MTDATA, the holes transportation in devices C and D improve with respect to device B which leads to the unbalanced injection and transportation of holes. Therefore the anode current and driving voltage in a given current can be improved in devices C and D than device B while the luminescent power and operating voltage in a given luminescent for device B are better than those for devices C and D. In comparison between devices C and D, due to the higher effective hole mobility of TPD in a typical applied biases than NPB, the holes transportation in device C can be improved than device D which leads to the unbalanced hole injection and transportation. Therefore the anode current and driving voltage in a given current can be improved in device C than device D while the luminescent power and operating voltage in a given luminescent power for device D are better than those for device C. Therefore among devices B, C and D, the driving voltage for device C is the lowest and for device B is the highest, while the operating voltage for device B is the lowest and for device C is the highest. In device E, due to the insertion of Alq_3 as ETL and increasing of the electron injection and transportation, the reduction of anode current and increasing of the driving voltage than other devices can be achieved. In this device, the carriers balance, lead to the increasing luminance and decreasing operating voltage than device A. In device F, with insertion of the m-MTDATA as HTL and Alq3 as ETL, hole and electron injection and transportation can be markedly increased. In conclusion the driving voltage at a given current density and operating voltage at a given luminance power can be reduced that leads to the improvement of carrier balance, current density and luminance power than devices A and E. Therefore among all of the structures under study in this manuscript, the PLED device with the m-MTDATA (40 nm) layer as HTL (device B) has the best performance because of its best I-V and emission characteristics.

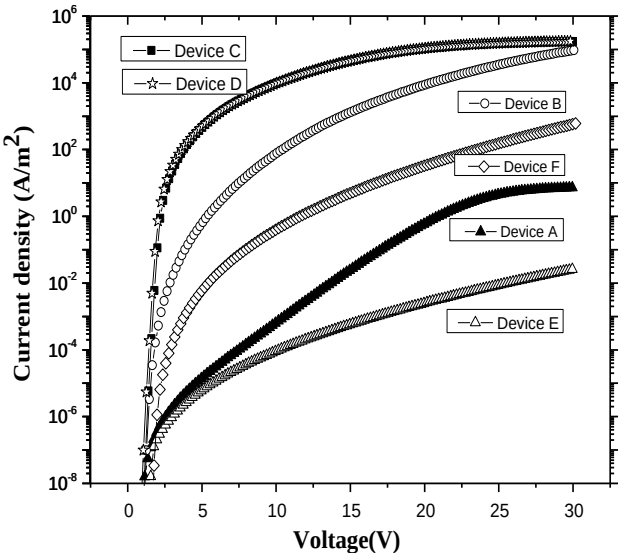

Fig. 5. Current density versus voltage

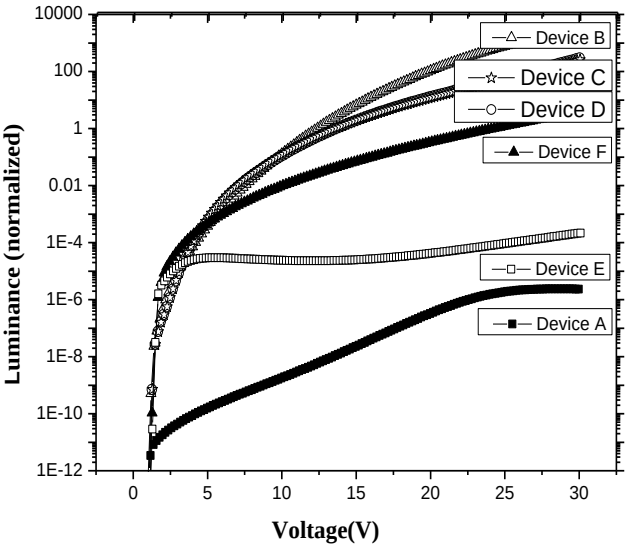

Fig. 6. Luminance versus voltage

Another point is that, the internal energy barriers (unequal LUMO or HOMO levels in two adjacent layers) lead to the accumulation of electrons and holes at the two layers interface. In conclusion a redistribution of the electric field can be achieved in devices. Fig. 7 shows the electric field distributions at different layers of PLEDs devices under study in this manuscript. As can be seen from these figures, in device A due to the accumulation of electrons and holes at the EML, the maximum charge concentration and maximum electric field can be achieved in this layer. In device B, the accumulation of holes at the HTL/EML interface lead to the maximum charge concentration in this interface. In conclusion, due to the lowest effective mobility of charge carriers in Ph-PPV layer, the maximum electric field is observed in the EML. In devices C and D, the accumulation of holes at the m-MTDATA/TPD and m-MTDATA/NPB interfaces leads to

the maximum charge concentration in these interfaces. In conclusion due to the lowest effective mobility of charge carriers at typical applied biases in Ph-PPV layer, the maximum electric field can be achieved in the EML. In device E, the accumulation of electrons and holes at the Ph-PPV/Alq_3 interface lead to the maximum charge concentration in this interface. In conclusion, due to the low effective mobility at typical applied biases in Alq_3 and Ph-PPV layers, the maximum electric field is observed in these layers. In device F, the accumulation of holes at the m-MTDATA/Ph-PPV and Ph-PPV/Alq_3 interfaces and electrons at the m-MTDATA/Ph-PPV interface lead to the maximum charge concentration in Ph-PPV/Alq_3 interface. In conclusion, due to the lowest effective mobility at typical applied biases in Alq_3 layer, the maximum electric field is observed in this layer.

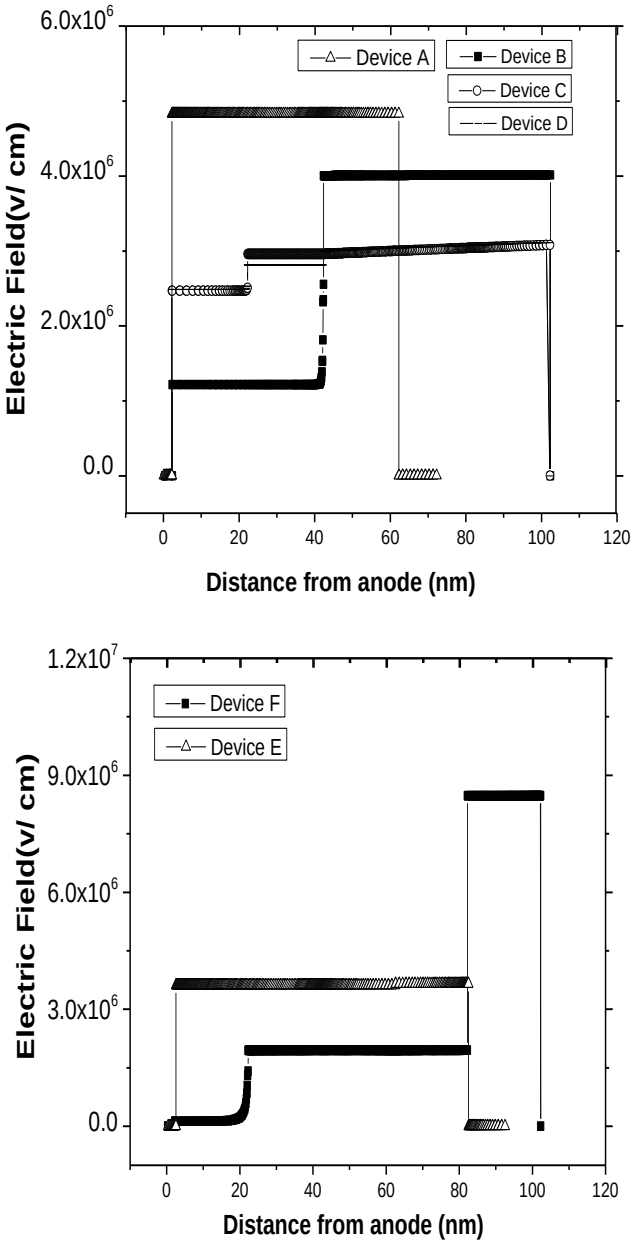

Fig. 7. Electric field versus distance from anode

6. Conclusion

In single layer PLED devices which have been constituted from only an EML, the insertion of other organic materials between anode and cathode as HTL and ETL lead to the modification of imbalanced injection and imbalanced transportation of electrons and holes. In conclusion, the recombination zone shifts away from the electrodes and luminescence quenching is avoided. In fact organic materials used as HTL and ETL in PLED structures lead to the balanced charge carriers injection and transportation and in conclusion the increased recombination rate can be achieved in the active layer. This leads to the improvement of luminance power and performance in these devices due to the effective parameters of organic materials (affinity, band gap and mobility). In device A, the constant recombination rate of electrons and holes in the EML leads to the exciton profile with a maximum in this layer and a tail in the contacts. In other devices, the highest recombination rate of electrons and holes in the HTL/EML or EML/ETL interfaces leads to the singlet exciton density profile with a maximum in these interfaces and a tail in other regions. In fact, in device A, the unbalanced injection and transportation of electrons and holes causes the device to perform poorly. The insertion of m-MTDATA, m-MTDATA/TPD and m-MTDATA/NPB as hole transport layer (HTL) and Alq_3 as electron transport layer (ETL) in other devices improves the situation of charge carriers balance and leads to the better performance for these devices with respect to device A. In comparison between all devices under investigation in this manuscript, the PLED device with m-MTDATA layer (40 nm) as HTL (device B) has the best performance.

References

[1] Herman T. Nicolai, Andre Hof, Jasper L. M. Oosthoek, Paul W. M. Blom, Adv. Funct. Mater. **21**, 1505 (2011).

[2] P. Yam, Polymer Electronics. Sci. Am. **273**, 74 (1995).

[3] H. Shirakawa, E. J. Louis, A. G. Macdiarmid, K. Chiang, A. J. Heeger, X. J. Chem, Chem. Commun. **16**, 578 (1977).

[4] C. W. Tang, S. A. Vanslyke, Appl. Phys. Lett. **51**, 913 (1987).

[5] Li Wang, Wei Xu, Yu Luo, Junwen Yuan, Yucheng Ding, Displays **32**, 45 (2011).

[6] L. C. Meng, Z. D. Lou, S. Y. Yang, Y. B. Hou, F. Teng, X. J. Liu, Y. B. Li, Chin. Phys. B **16**, 624 (2012).

[7] J. H. Burroughes, D. D. C. Bradley, A. R. Brown, R. N. Marks, K. Mackay, R. H. Friend, P. L. Burns, A. B. Holmes, Nature (London) **347**, 539 (1990).

[8] A. H. Reshak, M. M. Shahimin, N. Juhari, S. Suppiah, Progress in Biophysics and Molecular Biology **113**, 289 (2013).

[9] K. Lee, J. Y. Kim, S. H. Park, S. H. Kim, S. Cho, A. J. Heeger, Adv. Mater. **19**, 2445 (2007).

[10] J. C. Scott, G. G. Malliaras, Chem. Phys. Lett. **299**, 115 (1999).
[11] B. K. Crone, P. S. Davids, I. H. Campbell, D. L. Smith, J. Appl. Phys. **87**, 1974 (2000).
[12] H. Bassler, Phys. Status Solidi B **175**, 15 (1993).
[13] H. Houili, E. Tutis, H. Lutjens, M. N. Bussac, L. Zuppiroli, Comput. Phys. Commun. **156**, 108 (2003).
[14] R. Coehoorn, S. L. M. van Mensfoort, Phys. Rev. B **80**, 085302 (2009).
[15] S. L. M. van Mensfoort, R. Coehoorn, Phys. Rev. B **78**, 085207 (2008).
[16] S. Lee, H. Koo, O. Kwon, Y. J. Park, H. Choi, K. Lee, B. Ahn, Y. M. Park, Sci. Rep. **7**, 11995 (2017).
[17] S. J. Martin, A. B. Walker, A. J. Campbell, D. D. C. Bradley, J. Appl. Phys. **98**, 063709 (2005).
[18] W. Brutting, S. Berleb, A. G. Muckl, Organic Electron. **2**, 1 (2001).
[19] B. Ruhstaller, T. Beierlein, H. Riel, S. Karg, J. C. Scott, W. Riess, IEEE J. Select. Topics Quantum Electron **9**, 723 (2003).
[20] S. M. Sze, Physics of Semiconductor Devices, 2nd ed. New York, NY, USA: Wiley (1981).
[21] G. G. Malliaras, J. C. Scott, J. Appl. Phys. **85**, 7426 (1999).
[22] C. M. Wu, E. S. Yang, Solid-State Electronics **22**, 241 (1979).
[23] K. Yang, J. East, G. Haddad, Solid-State Electronics **36**, 321 (1993).
[24] D. Nayak, R. B. Choudhary, Microelectronics Reliability **144**, 114959 (2023).
[25] N. Patel, S. Cina, J. Burroughes, IEEE J. Sel. Top. Quantum Eletron. **8**, 346 (2002).
[26] G. Horowitz, Adv. Mater. **10**, 365 (1998).
[27] B. Ruhstaller, S. A. Carter, S. Barth, H. Riel, W. Riess, J. Appl. Phys. **89**, 4575 (2001).
[28] H. Siemund, H. Gobel, IEEE. Trans. Elect. Device **63**, 9 (2016).
[29] D. Das, P. Gopikrishna, D. Barman, R. B. Yathirajula, P. K. Lyer, Nano Convergence **6**, 31 (2019).
[30] S. Barth, P. Muller, H. Riel, P. F. Seidler, W. Rie, H. Vestweber, H. Bassler, J. Appl. Phys. **89** (2001).
[31] S. Schols, S. Verlaak, C. Rolin, D. Cheyns, J. Genoe, P. Heremans, Adv. Funct. Mater. **18**, 136 (2008).
[32] S. W. Liu, J. H. Lee, C. C. Lee, C. T. Chen, J. K. Wang, Appl. Phys. Lett. **91**, 142106 (2007).
[33] L. Duan, H. Li, Y. Qiu, J. Phys. Chem. C **118**(51), 29636 (2014).
[34] M. L. Chen, C. H. Yang, C. Y. Wen, S. H. Chang, Y. K. Kuo, Proc. of SPIE **6655**, 66551T-1 (2007).
[35] B. S. Mohammed, N. E. Chabane Sari, M. K. Selma, Trans. Electr. Electron. Mater. **16**(3), 124 (2015).
[36] Dheeraj K. Mohata, Durgesh C. Tripathi, Y. N. Mohapatra, Proceedings of MRS Fall Meeting **1115**, 68 (2008).
[37] H. Siemund, F. Bröcker, H. Göbel, Organic Electronics **14**, 335 (2013).
[38] G. Paasch, A. Nesterov, S. Scheinert, Synthetic Metals **139**, 425 (2003).
[39] H. Siemund, H. Gobel, IEEE Trans on Electron. Devices **63**, 9 (2016).
[40] D. Das, P. Gopikrishna, R. Narasimhan, A. Singh, A. Dey, P. K. Iyer, Phys. Chem. Chem. Phys. **18**(48), 33077 (2016).
[41] D. Das, P. Gopikrishna, D. Barman, R. B. Yathirajula, P. K. Iyer, Journal of Physics and Chemistry of Solids **163**, 110577 (2022).
[42] D. H. Rose, R. E. Bank, Numerische Mathematik **37**, 279 (1981).
[43] C. H. Price, Ph. D. Dissertation, Stanford University (1982).

*Corresponding author: auobi_ali@yahoo.com